Journal of Industrial and Engineering Chemistry 87 (2020) 213–221

Contents lists available at ScienceDirect

Journal of Industrial and Engineering Chemistry

journal homepage: www.elsevier.com/locate/jiec

High electroluminescence efficiency and long device lifetime of a fluorescent green-light emitter using aggregation-induced emission

Hyocheol Jung[a,b], Hwangyu Shin[c], Siin Kim[d,e], Joonghan Kim[c], Byeong-Kwan An[c], Ji-Hoon Lee[a], Hyotcherl Ihee[d,e], Jongwook Park[b,*]

[a] Department of Polymer Science and Engineering, Korea National University of Transportation, 50 Daehak-ro, Chungju-si, Chungbuk 27909, Republic of Korea
[b] Department of Chemical Engineering, Kyung Hee University, Gyeonggi-do 17104, Republic of Korea
[c] Department of Chemistry, Catholic University of Korea, Bucheon 14662, Republic of Korea
[d] Department of Chemistry and KI for the BioCentury, Korea Advanced Institute of Science and Technology (KAIST), Daejeon 34141, Republic of Korea
[e] Center for Nanomaterials and Chemical Reactions, Institute for Basic Science (IBS), Daejeon 34141, Republic of Korea

ARTICLE INFO

Article history:
Received 30 January 2020
Received in revised form 10 March 2020
Accepted 2 April 2020
Available online 19 April 2020

Keywords:
Organic light-emitting diodes
Fluorescence
Green emitter
Aggregation-induced emission
Luminance efficiency
Device lifetime

ABSTRACT

Three bipolar materials, 4-(4,6-diphenyl-1,3,5-triazin-2-yl)-N,N-diphenylaniline (DPAT-Ph), 4-(4,6-diphenyl-1,3,5-triazin-2-yl)-N,N-diphenylnaphthalen-1-amine (DPAT-Na), and 10-(4,6-diphenyl-1,3,5-triazin-2-yl)-N,N-diphenylanthracen-9-amine (DPAT-An), were designed and synthesized. To achieve a bipolar character, diphenylamine (DPA) moiety and 2,4-diphenyl-1,3,5-triazine (DPT) moiety were introduced as electron donating and electron accepting groups, respectively. The three compounds exhibited UV maximum wavelengths (UV_{max}) at 395–454 nm and photoluminescence maximum wavelengths (PL_{max}) at 472–546 nm. 10-(4,6-Diphenyl-1,3,5-triazin-2-yl)-N,N-diphenylanthracen-9-amine (DPAT-An) shows AIE phenomenon even though DPAT-An does not have tetraphenylethylene (TPE) moiety which is representative AIE structure. DPAT-An exhibits over EQE value of 5% and long device lifetime of 1310 h without sublimation process.

Introduction

π-Conjugated organic materials have been applied to a variety of fields and have been continually developed. There are many reports related to optoelectronic fields such as organic light-emitting diodes (OLEDs), solar cells, and organic thin-film transistors [1–3]. Since Tang and Van Slyke reported on OLEDs in 1987, OLEDs have attracted great interest because of their potential in full-color flat panel display applications [4–7]. To be used OLEDs in a variety of applications such as mobile phones and televisions, emitters with both high efficiency and a long lifetime need to be developed.

Most materials used as the emitter in an OLED device are π-conjugated organic materials, which involve an intrinsic issue. Generally, π-conjugated organic materials exhibit strong photoluminescence (PL) intensity in the dilute solution state, while in the concentrated solution state, solid state, or film state, PL intensity decreases because PL quenching occurs due to the strong π–π interactions between molecules [11].

To prevent PL quenching by intermolecular π–π interaction and develop emitters with high efficiency and long device lifetime, we have designed and synthesized molecules based on the core-side concept. The core group plays a basic role in determining the emission wavelength and photoluminescence quantum yield (PLQY) of emitters. The side group bonded to the core group controls the molecular structure, orientation, and polarity, which can prevent excimer emission, fine-tune emission wavelength, and increase PLQY. Based on this concept, there are many results of OLED devices with high performances used chromophores with high PLQY as core group and ter-phenyl or electron donating group such as diphenylamine (DPA) moiety and triphenylamine (TPA) moiety as side group [8–10].

In 2001, Tang's group reported on the aggregation-induced emission (AIE) phenomenon, which can overcome the issue of PL quenching by intermolecular π–π interaction [11]. Emitters exhibiting the AIE phenomenon exhibit a weak PL intensity in the dilute solution state because non-radiative decay such as molecular vibrational and rotational motions is dominant. However, in the concentrated solution state or solid state, the emitters exhibit a strong PL intensity because radiative decay is dominant due to restriction of intramolecular motions (RIM). Therefore, the AIE phenomenon could help increase the

* Corresponding author.
E-mail address: jongpark@khu.ac.kr (J. Park).

https://doi.org/10.1016/j.jiec.2020.04.003
1226-086X/

electroluminescence (EL) efficiency of OLED devices which operate in thin film state [12]. There are many reports on high-performing OLED devices that are based on AIE molecules [13–18].

To achieve high EL performances, charge transport and charge balance are important [19–21]. Bipolar emitters, which have both an electron donating group and an electron accepting group in the same molecule, can satisfy these factors. Because the bipolar concept not only balances charge carriers, but also widens the charge recombination zone, the EL performance of OLED devices can be increased [22,23].

In this study, the phenyl, naphthyl, and anthracene are selected for the core group. To create a bipolar characteristic in the final molecules, diphenylamine (DPA) moiety and 2,4-diphenyl-1,3,5-triazine (DPT) moiety were selected as electron donating and electron accepting side groups, respectively. We report the change in characteristics and EL performances of OLED devices caused by different core groups located between the same bipolar side groups. Especially, only 10-(4,6-diphenyl-1,3,5-triazin-2-yl)-N,N-diphenylanthracen-9-amine (DPAT-An) shows AIE phenomenon even though DPAT-An does not have tetraphenylethylene (TPE) moiety which is representative molecular structure of AIE phenomenon. Also, in EL performances, DPAT-An exhibits over EQE value of 5% and long device lifetime of 1310 h without sublimation process.

Experimental

General information

The ^{1}H-NMR spectra and ^{13}C-NMR spectra were recorded on Bruker Avance 300 and Avance 500 spectrometers. The FAB^{+}-mass and EI^{+}-spectra were recorded on a JEOL JMS-AX505WA, HP5890 series II. The optical absorption spectra were obtained using a Lambda 1050 UV/Vis/NIR spectrometer (PerkinElmer). A PerkinElmer luminescence spectrometer LS50 (xenon flash tube) was used to perform PL spectroscopy. UV–vis absorption maximum wavelength values of solution state and film state were selected as the excitation wavelength values for PL measurement in solution and film states, respectively. Absolute PLQY were measured using a QM-400 spectrofluorometer (Horiba). T_g values of the compounds were determined under a nitrogen atmosphere with a DSC4000 (PerkinElmer). Samples were heated to 360 or 400 °C at a rate of 10 °C min^{-1}, cooled at 10 °C min^{-1}, and then heated again under the same conditions as in the initial heating process. T_d values were determined with a TGA4000 (PerkinElmer). Samples were heated to 800 °C at a rate of 10 °C min^{-1}.

The HOMO energy levels were determined with ultraviolet photoelectron yield spectroscopy (Riken Keiki AC-2). The LUMO energy levels were derived from the HOMO energy levels and the band gaps. The optimized molecular structures were obtained by DFT with the Gaussian09 program [24].

In each of the EL devices, ITO was used as the anode and Al as the cathode. All organic layers were deposited under 10^{-6} Torr, with a rate of deposition of 1 Å s^{-1} to create an emitting area of 4 mm^2. The LiF and aluminum layers were continuously deposited under the same vacuum conditions. The luminance efficiency data for the fabricated EL devices were obtained with a Keithley 2400 electrometer. Light intensities were obtained with a Minolta CS-1000A. The operational stabilities of the devices were measured while encapsulated and in a glove box. The device lifetimes were determined using the Polaronix OLED Lifetime Test System of McScience.

Synthesis

(1) Synthesis of compound 2

Compound 1 (2 g, 6.17 mmol) was added to 70 mL of anhydrous tetrahydrofuran (THF) and stirred at −78 °C, and then 2.0 M n-BuLi (3.70 mL, 7.40 mmol) was added. After 30 min of stirring, triethyl borate (1.46 mL, 8.64 mmol) was added to the reaction mixture. After the reaction was finished, the solution was acidified with a 2 N HCl solution at room temperature and extracted with ethyl acetate (EA) and H_2O. The organic layer was dried with anhydrous $MgSO_4$ and filtered. The solvent was evaporated. The residue was re-dissolved in THF and added to *n*-hexane. The precipitation was filtered and washed with hexane to obtain a gray product (1.05 g, yield 60%). ^{1}H-NMR (300 MHz, $CDCl_3$): δ (ppm) 8.02 (d, 1H), 7.32 (m, 2H), 7.16 (m, 2H), 7.06 (m, 2H), 1.53 (s, 2H).

(2) Synthesis of DPAT-Ph (I)

Compound 3 (1.0 g, 3.61 mmol) and tetrakis(triphenylphospine) palladium(0) ($Pd(PPh_3)_4$) (0.20 g, 0.18 mmol) were added to 30 mL of anhydrous toluene. Then, 9 mL of a 2 M Na_2CO_3 (aq) solution was added to the reaction mixture, followed by addition of compound 2 (1.25 g, 4.33 mmol). The reaction mixture was heated to 85 °C for 10 h under nitrogen. After the reaction was finished, the reaction mixture was extracted with $CHCl_3$ and H_2O. The organic layer was dried with anhydrous $MgSO_4$ and filtered. The solvent was evaporated. The product was purified by column chromatography with an eluent of 1:3 $CHCl_3$/*n*-hexane. The solvent was evaporated. The residue was re-dissolved in THF and added to ethanol. The precipitation was filtered and washed with ethanol to obtain a gray solid (yield 26%). ^{1}H-NMR (300 MHz, $CDCl_3$): δ (ppm) 8.77–8.73 (m, 2H), 8.63–8.58 (d, 1H), 7.62–7.52 (m, 3H), 7.35–7.29 (t, 2H), 7.22–7.10 (m, 4H). ^{13}C-NMR (75 MHz, $CDCl_3$): δ (ppm) 171.6, 171.4, 152.1, 147.2, 136.7, 132.5, 130.4, 129.7, 129.1, 129.0, 128.8, 125.9, 124.4, 121.2. HRMS (EI, *m*/*z*): $[M]^+$ calcd for $C_{33}H_{24}N_4$, 476.2001; found, 476.2001. Anal. calcd for $C_{33}H_{24}N_4$: C 83.17, H 5.08, N 11.76; found: C 81.81, H 5.18, N 11.35.

(3) Synthesis of compound 6

Compound 5 (2.53 g, 8.85 mmol), compound 4 (1.36 g, 8.05 mmol), sodium *tert*-butoxide (1.55 g, 16.1 mmol), tris(dibenzylideneacetone)dipalladium(0) ($Pd_2(dba)_3$, 0.074 g, 0.081 mmol), and 2,2′-bis(diphenylphosphino)-1,1′-binaphhtyl (BINAP) (0.040 g, 0.064 mmol) were added to 250 mL of anhydrous toluene. The reaction mixture was refluxed for 8 h under nitrogen. After the reaction was finished, the reaction mixture was extracted with $CHCl_3$ and H_2O. The organic layer was dried with anhydrous $MgSO_4$ and filtered. The solvent was evaporated. The product was purified using column chromatography with an eluent of 1:3 $CHCl_3$/*n*-hexane. The solvent was evaporated. The residue was re-dissolved in $CHCl_3$ and added to methanol. The precipitation was filtered and washed with methanol to obtain a white solid (0.50 g, yield 17%). ^{1}H-NMR (300 MHz, $CDCl_3$): δ (ppm) 8.27–8.24 (d, 1H), 7.98–7.95 (d, 1H), 7.77–7.75 (d, 1H), 7.59–7.53 (t, 1H), 7.42–7.37 (t, 1H), 7.21–7.15 (m, 5H), 7.02–6.96 (d, 4H), 6.95–6.91 (t, 2H).

(4) Synthesis of compound 7

Compound 6 (0.5 g, 1.34 mmol) was added to 15 mL of anhydrous THF and stirred at −78 °C, then 2.0 M n-BuLi (1.00 mL, 1.61 mmol) was added. After 30 min of stirring, isopropoxy-4,4,5,5-tetramethyl-1,3,2-dioxaborolane (0.38 mL, 1.88 mmol) was added to the reaction mixture. After the reaction was finished, the product was extracted with $CHCl_3$ and H_2O. The organic layer was dried with anhydrous $MgSO_4$ and filtered. The solvent was evaporated. The product was purified with column chromatography with an eluent of 1:3 $CHCl_3$/*n*-hexane. The solvent was evaporated. The residue was re-dissolved in $CHCl_3$ and added to methanol. The precipitation was filtered and washed with methanol to obtain a beige solid (5.0 g, yield 54.6%). ^{1}H-NMR (300 MHz, $CDCl_3$): δ (ppm) 7.87 (d, 2H), 7.22 (m, 4H), 7.10 (m, 6H), 6.97 (t, 2H), 1.32 (s, 12H).

(5) Synthesis of DPAT-Na (II)

Compound 7 (0.3 g, 0.71 mmol), compound 3 (0.22 g, 0.85 mmol), palladium(II) acetate ($Pd(OAc)_2$, 0.005 g, 0.021 mmol), and tricyclohexylphosphine ($(cyclohexyl)_3P$, 0.012 g, 0.043 mmol) were added to anhydrous THF (30 mL). Then tetraethylammonium hydroxide (20 wt%, 0.3 mL, 2.14 mmol) was added to the reaction mixture at 60 °C. The mixture was refluxed for 12 h under nitrogen. After the reaction was finished, the reaction mixture was extracted with $CHCl_3$ and H_2O. The organic layer was dried with anhydrous $MgSO_4$ and filtered. The solvent was evaporated. The reaction mixture was purified by column chromatography with an eluent of 1:4 $CHCl_3$/n-hexane to yield a yellowish green solid (0.20 g, yield 53%). ^{1}H NMR (300 MHz, THF-d_8): δ (ppm) 9.21 (d, 1 H), 8.80–8.77 (m, 4H), 8.53 (d, 1H), 8.11 (d, 1H), 8.08–7.55 (m, 7H), 7.46–7.42 (m, 2H), 7.23–7.21 (m, 4H), 7.10 (d, 4H), 7.02 (t, 2H); ^{13}C-NMR (75 MHz, $CDCl_3$): δ (ppm) 174.4, 171.8, 148.7, 147.9, 136.4, 133.5, 132.9, 131.9, 131.7, 129.5, 129.3, 129.0, 127.6, 126.8, 126.6, 126.2, 125.3, 122.8, 122.5; HRMS (EI, *m*/*z*): $[M]^+$ calcd for $C_{37}H_{26}N_4$, 526.2157; found, 526.2145. Anal. Calcd for $C_{37}H_{26}N_4$: C 84.38, H 4.98, N 10.64; found: C 83.16, H 5.07, N 10.27.

(6) Synthesis of compound 8

9-Bromoanthracence (10.0 g, 38.9 mmol) was dissolved in anhydrous THF (500 mL) and stirred at −78 °C. Then, 1.6 M *n*-butyllithium (n-BuLi, 29.3 mL, 46.7 mmol) was added. Triethyl borate (9.3 mL, 54.5 mmol) was added to the reaction after 30 min. After the reaction was finished, the solution was acidified with a 2 N HCl (aq) solution at room temperature and extracted with EA and H_2O. The organic layer was dried over anhydrous $MgSO_4$ and filtered. The solvent was evaporated. The residue was re-dissolved in EA, and *n*-hexane was added into the solution. The precipitate was filtered and washed with *n*-hexane to obtain a beige solid (7.70 g, yield 89%). ^{1}H-NMR (300 MHz, $CDCl_3$): δ (ppm) 8.47 (s, 1H), 8.14 (d, J = 9.2 Hz, 2H), 8.04 (d, J = 9.8 Hz, 2H), 7.53–7.44 (m, 4H), 5.07 ppm (s, 2H).

(7) Synthesis of compound 9

Compound 3 (4.0 g, 15.0 mmol), compound 8 (1.25 g, 4.33 mmol), and $Pd(PPh_3)_4$ (0.20 g, 0.18 mmol) were added to 150 mL of anhydrous toluene and 16 mL of anhydrous ethanol. Then, 9 mL of a 2 M Na_2CO_3 (aq) solution was added to the reaction mixture. The reaction mixture was refluxed for 10 h under nitrogen. After the reaction was finished, the reaction mixture was extracted with $CHCl_3$ and H_2O. The organic layer was dried with anhydrous $MgSO_4$ and filtered. The solvent was evaporated. The product was purified by column chromatography with an eluent of 1:3 dicloromethane/*n*-hexane. The solvent was evaporated. The residue was re-dissolved in THF and added to methanol. The precipitation was filtered and washed with methanol to obtain a beige solid (yield 26%). ^{1}H-NMR (300 MHz, $CDCl_3$): δ (ppm) 8.77–8.73 (m, 2H), 8.63–8.58 (d, 1H), 7.62–7.52 (m, 3H), 7.35–7.29 (t, 2H), 7.22–7.10 (m, 4H).

(9) Synthesis of compound 10

Compound 9 (1.0 g, 2.19 mmol) and N-bromosuccinimide (NBS) (0.43 g, 2.41 mmol) were added to $CHCl_3$ (30.0 mL), and acetic acid (5.0 mL) was added to the reaction mixture. The mixture was refluxed for 2 h. After the reaction had finished, the reaction mixture was extracted with $CHCl_3$ and H_2O. The organic layer was dried over anhydrous $MgSO_4$ and filtered. The solution was evaporated. The residue was re-dissolved in ethanol and added to $CHCl_3$. The precipitate was filtered and washed with ethanol to obtain a yellow solid (1.1 g, yield 96%). ^{1}H-NMR (300 MHz, $CDCl_3$): δ (ppm) 8.75–8.71 (d, 4H), 8.68–8.65 (d, 2H), 7.83–7.80 (d, 2H), 7.65–7.59 (t, 4H), 7.56–7.51 (t, 4H), 7.48–7.43 (t, 2H).

(9) Synthesis of DPAT-An (III)

Compound 10 (1 g, 2.05 mmol), compound 4 (0.41 g, 2.46 mmol), sodium *tert*-butoxide (0.6 g, 6.15 mmol), $Pd_2(dba)_3$ (0.06 g, 0.061 mmol), and tri-*tert*-butylphosphine ($(t\text{-}Bu)_3P$, 0.07 mL, 0.31 mmol) were added to 100 mL of dry toluene. The reaction mixture was refluxed for 5 h under nitrogen. After the reaction was finished, the reaction mixture was extracted with $CHCl_3$ and H_2O. The organic layer was dried with anhydrous $MgSO_4$ and filtered. The solvent was evaporated. The product was isolated with silica gel column chromatography using an eluent of 1:3 $CHCl_3$/*n*-hexane. The solvent was removed by evaporation. The residue was re-dissolved in THF and added to ethanol. The precipitation was filtered and washed with methanol to obtain a yellow solid (0.46 g, yield 39%). ^{1}H NMR (300 MHz, $CDCl_3$): δ (ppm) 8.78–8.74 (d, 4H), 8.25–8.22 (m, 2H), 7.94–7.90 (m, 2H), 7.66–7.53 (m, 2H), 7.43–7.37 (m, 4H), 7.23–7.14 (m, 8H), 6.94–6.88 (t, 2H). ^{13}C-NMR (75 MHz, $CDCl_3$): δ (ppm) 175.9, 172.3, 147.9, 139.6, 136.0, 133.2, 132.6, 131.0, 130.8, 129.6, 129.5, 129.0, 129.0, 126.9, 126.8, 126.5, 125.0, 121.6, 120.7. HRMS (EI, *m*/*z*): $[M]^+$ calcd for $C_{41}H_{28}N_4$, 576.2314; found, 526.2310. Anal. Calcd for $C_{41}H_{28}N_4$: C 85.39, H 4.89, N 9.72; found: C 84.60, H 5.41, N 9.13.

Results and discussion

Synthesis and characterization

Scheme 1 shows the molecular structures of the synthesized compounds, 4-(4,6-diphenyl-1,3,5-triazin-2-yl)-N,N-diphenylaniline (DPAT-Ph), 4-(4,6-diphenyl-1,3,5-triazin-2-yl)-N,N-diphenylnaphthalen-1-amine (DPAT-Na), and DPAT-An. All three compounds contained the DPA moiety for donating electrons and the DPT moiety for accepting electrons, with the core group between them. Therefore, when the dipole moments that push and pull electrons were applied to the different cores with the same magnitude of force, the changes of characteristics on the effect of core type were observed and compared. All compounds were synthesized by boronylation, bromination, Suzuki aryl-aryl coupling reaction, or Buchwald–Hartwig amination, and Scheme 2 shows the synthetic routes of each compound. The synthesized compounds were purified by reprecipitation and column chromatography and were characterized by ^{1}H-NMR and ^{13}C-NMR spectroscopy, elemental analysis, and Fab-Mass analysis. The detailed synthetic method and results are explained in the Experimental.

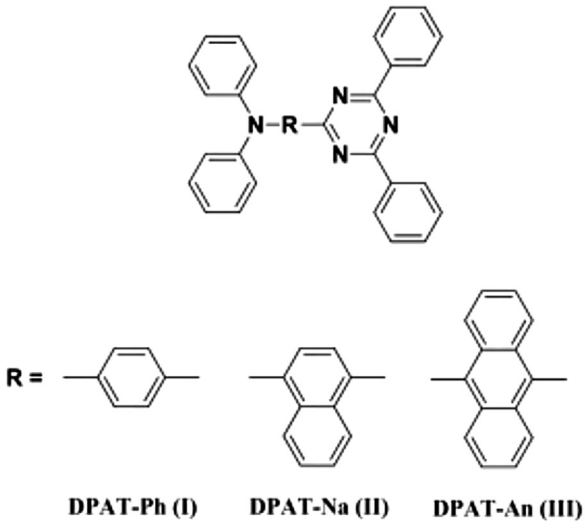

Scheme 1. Chemical structures of synthesized materials.

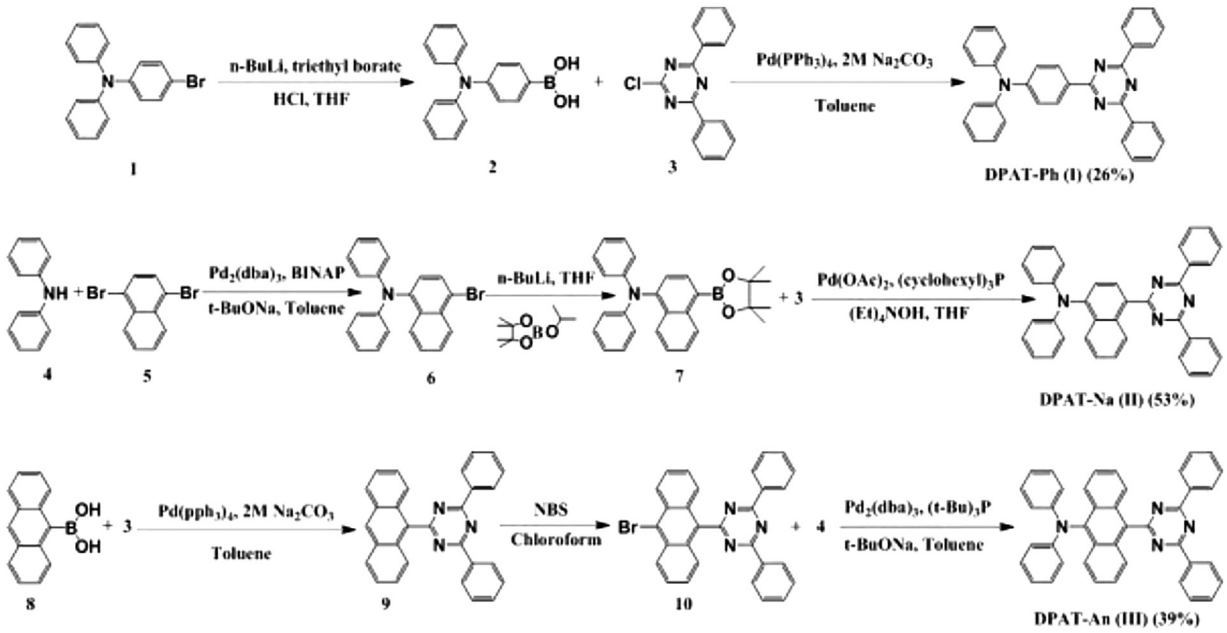

Scheme 2. Synthetic routes of synthesized compounds.

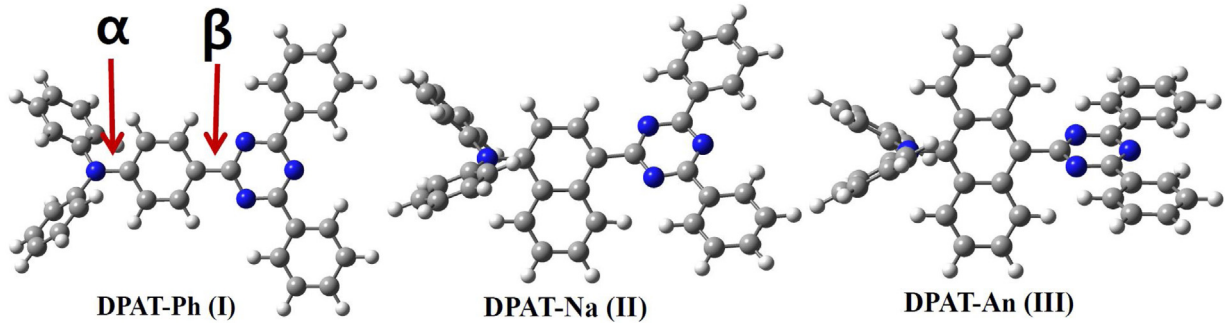

Fig. 1. Optimized molecular structures of synthesized DPAT-Ph, DPAT-Na, and DPAT-An (calculated by using CAMB3LYP/6-31G(d,p)).

Computational calculations

To confirm the optimized molecular structures, the structures of the three materials (DPAT-Ph, DPTA-Na, and DPAT-An) were calculated by density functional theory (DFT) based on CAMB3LYP/6-311G(d,p). Fig. 1 shows the optimized molecular structures of the synthesized compounds, and Table 1 shows the dihedral angles (α, β) of the compounds. α and β represent the dihedral angles between the core group and DPA moiety or DPT moiety, respectively. As the core group changed from phenyl to naphthyl to anthracene, α and β increased. The increase in dihedral angles was due to the increased repulsion between adjacent hydrogens in the molecule as the size of the core group increased from phenyl to anthracene. Among the three materials, DPAT-An, which had the most twisted molecular structure, efficiently can be prevented intermolecular π–π stacking in the film state and could exhibit relatively higher PLQY by decreasing PL quenching.

To predict the molecular packing structure of the three materials, dimer stacking models were calculated by ωB97XD/6-31G(d). In Fig. 2, dimer stacking structures of DPAT-Ph and DPAT-Na seem to be easy that core chromophores such as phenyl groups and naphthyl groups approach each other, which decreased absolute PLQY values by strong intermolecular π–π interaction. However, the angle of two anthracene moieties in case of DPAT-An is close to 90° and it is difficult for two anthracenes to approach each other in the dimer stacking structure of DPAT-An. This is because DPAT-An has the most twisted molecular structure. DPAT-An can exhibit a higher absolute PLQY value than those of DPAT-Ph and DPAT-Na by preventing intermolecular π–π interaction.

Table 1
Dihedral angles (α, β) of synthesized compounds calculated by CAMB3LYP/6-311G(d,p).

Dihedral angle	DPAT-Ph (I)	DPAT-Na (II)	DPAT-An (III)
α (°)	32	47	73
β (°)	0	30	63

Also, highest occupied molecular orbital (HOMO) and lowest unoccupied molecular orbital (LUMO) shapes of three materials are calculated by CAMB3LYP/6-31G(d,p). As seen in Fig. S3, electron density distributions of HOMO are located from DPA moiety to core chromophore, and electron density distributions of LUMO are located from DPT moiety to core chromophore. These electron density distributions exhibit bipolar characteristics.

Photophysical properties

To observe the effect of core groups on the optical properties, UV-Visible (UV–vis) absorption spectra and PL spectra were measured. Fig. 3 shows the UV–vis and PL spectra of the three

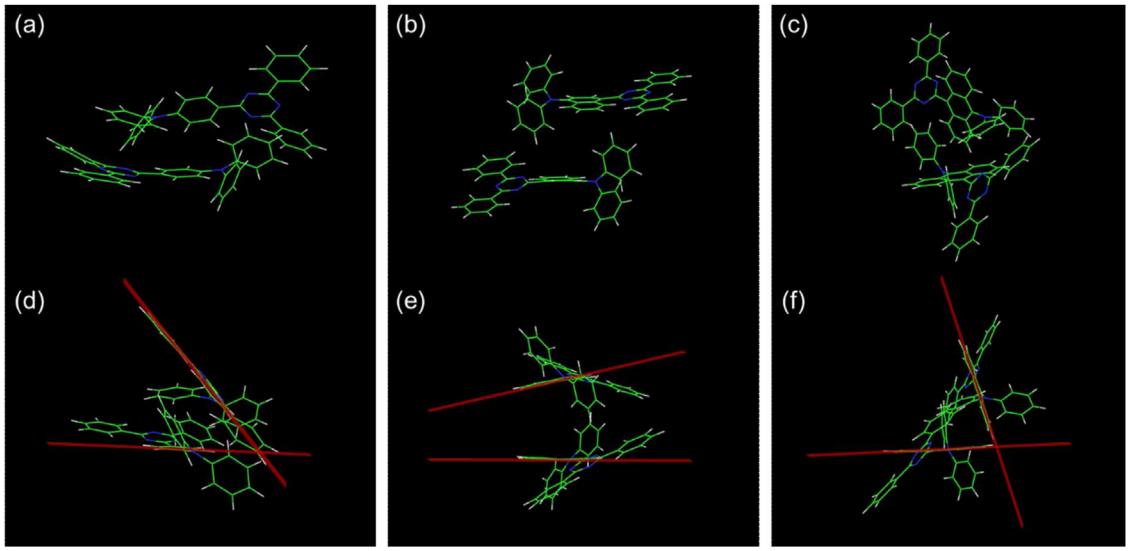

Fig. 2. Top: (front view) Optimized conformations of (a) DPAT-Ph, (b) DPAT-Na, and (c) DPAT-An dimers. Bottom: (side view) Optimized conformations of (d) DPAT-Ph, (e) DPAT-Na, and (f) DPAT-An dimers.

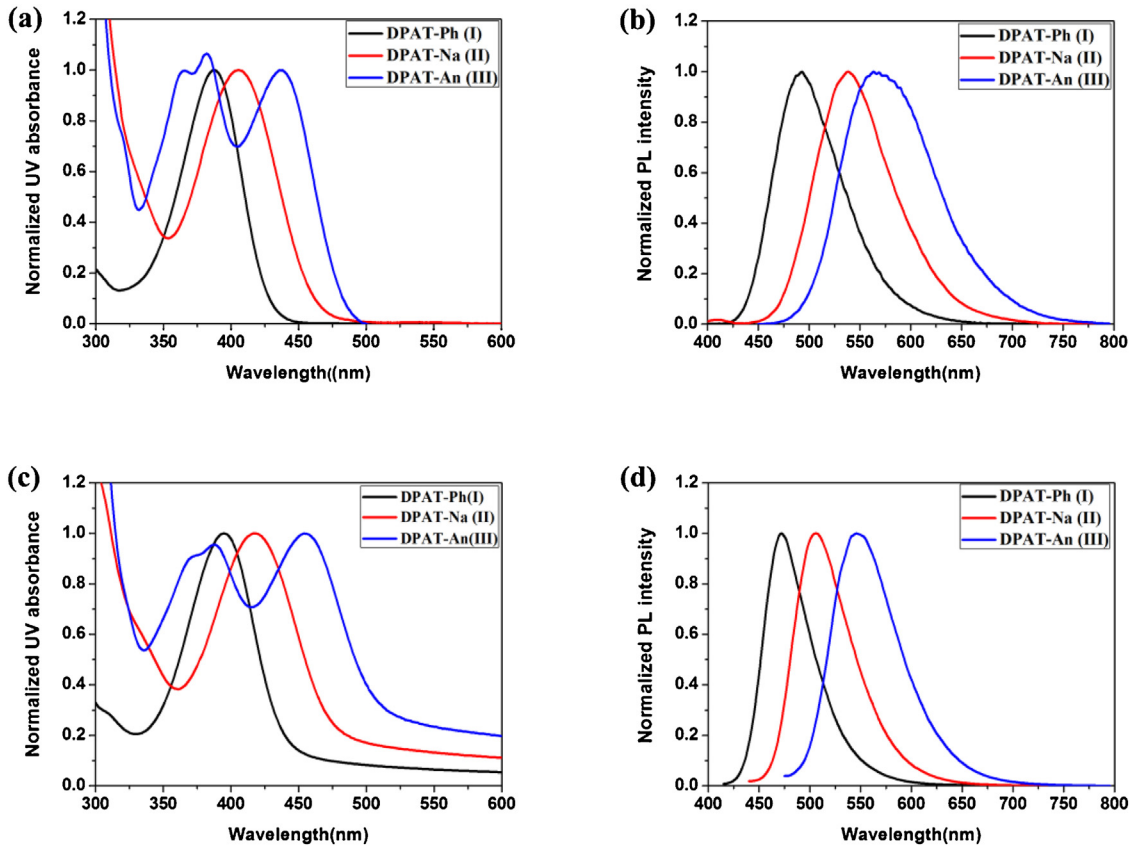

Fig. 3. UV–vis absorption spectra and PL spectra of synthesized compounds. (a,b) Spectra of synthesized compounds in solution in THF (1×10^{-5} M). (c,d) Spectra of the synthesized compounds in the thin film (solid) state prepared by thermal evaporation on glass.

materials in tetrahydrofuran (THF) solution and in thin film state. The optical data are summarized in Table 2 and Supporting information (Figs. S1, S2 and Tables S1 and S2). As seen in Fig. 3(a) and (c), the three synthesized materials exhibited UV–vis peaks in the range of 350–500 nm in solution and film state. Looking at the change of UV–visible absorption maximum (UV_{max}) peak, the three materials exhibit UV_{max} values of 388, 405, and 438 nm in solution state and UV_{max} values of 395, 417, and 454 nm in film state, respectively. Also, looking at the edge of UV–vis absorption spectra in the solution state, when the core was changed from phenyl to anthracene, the edge wavelength of the UV–vis spectrum was red-shifted to 437, 470, and 491 nm, respectively. When the core was changed from phenyl to anthracene in the film state, the edge wavelength of the UV–vis spectrum was red-shifted to 438, 473, and 505 nm, respectively. As a result, when the core group was changed from phenyl to anthracene, UV_{max} values were red-shifted

Table 2
Optical, electrochemical, and thermal properties of synthesized compounds.

Synthesized compounds	Film on glass		Φ_f (%)[a]		FWHM[c] (nm)	HOMO[d] (eV)	LUMO (eV)	Band gap (eV)	T_g (°C)	T_d (°C)
	λ^{ab}_{max} (nm)	λ^{em}_{max} (nm)	Solution[b]	Film[c]						
DPAT-Ph	395	472	79.7	53.8	55	−5.66	−2.83	2.83	68	342
DPAT-Na	417	506	78.7	44.5	65	−5.67	−3.05	2.62	89	365
DPAT-An	454	546	5.9	64.0	78	−5.65	−3.19	2.46	242	370

[a] Absolute photoluminescence quantum yield.
[b] In dilute toluene solution state.
[c] Thin film prepared by thermal evaporation.
[d] Ultraviolet photoelectron spectroscopy (Riken-Keiki, AC-2).

both in solution state and in film state. Likewise, in the case of the PL maximum wavelength (PL_{max}), the emission wavelength for DPAT-Ph, DPAT-Na, and DPAT-An was red-shifted to 490, 538, and 556 nm in solution state, and the emission wavelength was also red-shifted to 472, 506, and 546 nm in film state, respectively. This is because conjugation length of final molecule is lengthened when the conjugation length of core group is lengthened.

The three materials had a dipole moment by an electron donating and accepting group. Molecules with dipole moment have different optical properties depending on the solvent polarity. To evaluate the optical properties of three materials according to the solvent polarity, UV–vis and PL spectra were measured in different solvents (Figs. S1 and S2). As seen in the UV–vis absorption spectra, even though solvent polarity increased, the UV_{max} exhibited similar values. However, in the PL spectra, the PL_{max} values were gradually red-shifted with increasing solvent polarity. These red-shifts mean that the excited state related with PL emission was relatively affected by solvent polarity even though the dipole moment of the molecules was almost unaffected in the ground state. Because in the excited state, the dipole moment of molecules was stabilized according to the solvent polarity, the PLmax values were gradually red-shifted.

In the solution state and film states, the UV_{max} peaks exhibited intramolecular charge transfer (ICT). The charge transport direction of three molecules is started from DPA group to DPT group. As shown in Fig. 4, the slope order was DPAT-Ph > DPAT-Na > DPAT-An because of the different electron density at core groups such as benzene, naphthalene, and anthracene. To further understand the relationship between the three materials and the solvent, the Lippert-Mataga equation was used. As seen in Fig. 4, when the Stokes shift (y-axis) was plotted against orientation polarizability (x-axis), all three materials tended to increase linearly, showing that ICT efficiently occurred [25].

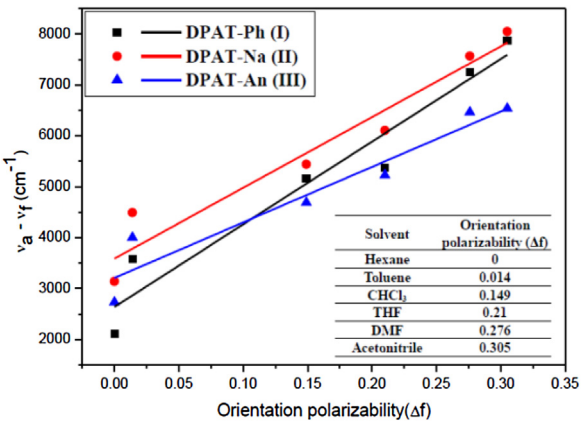

Fig. 4. Stokes shift ($\nu_a - \nu_f$) versus orientation polarizability (Δf) in different solvents to determine the solvent polarity parameter-photoluminescence λ_{max} fitting line. ν_a and ν_f are the wavenumber at maximum absorption and emission, respectively. Δf is calculated from the Lippert orientation polarizability function, $\Delta f = (\varepsilon - 1)/(2\varepsilon + 1) - (n^2 - 1)/(2n^2 + 1)$, where ε is dielectric constant, and n is refractive index.

Looking at the change of PL_{max} peaks in Fig. 3(b). and (d), the PL_{max} values of DPAT-Ph, DPAT-Na, and DPAT-An appeared at 490, 538, and 556 nm in a THF solution state, respectively. Also, these PL_{max} values appeared at 472, 506, and 546 nm in a film state, respectively. The PL_{max} values were red-shifted when the core group changed from phenyl to anthracene, which matched the trend of UV_{max} values.

In Table 2, one remarkable point is the absolute PLQY values of the three materials. In the solution state, the three materials exhibited an absolute PLQY value of 79.7%, 78.7%, and 5.9%, respectively, and exhibited an absolute PLQY value of 53.8%, 44.5%, and 64.0% in film state. In the case of DPAT-Ph and DPAT-Na, the absolute PLQY in the solution state exhibited higher PLQY values than the absolute PLQY in the film state. This was because PL quenching occurred by intermolecular packing in the film state, which is a general phenomenon exhibited by π-conjugated organic molecules. However, for DPAT-An the absolute PLQY value in the film state was about 11 times larger than in the solution state. To understand these results, a simple AIE test was performed for the three materials (Fig. 5.). The three materials can be dissolved in organic solvents such as toluene, chloroform, and THF, but cannot be dissolved in H_2O. After dissolving the three materials in THF, each material was solidified by adding H_2O, which did not dissolve the chromophore but could be well-mixed with THF. The change of PL intensity is plotted in Fig. 5. In the case of DPAT-Ph and DPAT-Na, the PL intensity in a THF 20%:H_2O 80% mixture was lower than that in 100% THF. However, in the case of DPAT-An, the PL intensity in THF 20%:H_2O 80% was higher than that in 100% THF. When the non-solvent H_2O was added to the good solvent THF, the solutes aggregated. In case of DPAT-Ph and DPAT-Na, PL quenching was occurred by intermolecular aggregation, while DPAT-An exhibited increased PL intensity by RIM process through intermolecular aggregation, which is typical AIE phenomenon [11]. Fig. 6 shows quantitative change of absolute PLQY value according to increase of water vol%. The absolute PLQY values were as low as 10–15% up to a water vol% of 40%. However, as water vol% increased to 60%, the absolute PLQY value began to increase, and the highest PLQY value of 64% was obtained at a water vol% of 80%. Because DPAT-An has the most twisted molecular structure, and molecular packing structure which can prevent intramolecular motions such as rotational and vibrational motion, DPAT-An only exhibited AIE phenomenon by RIM. Because the AIE phenomenon exhibits a higher PLQY value in the film state than in the solution state, it could help for increasing the EL efficiency of an OLED device.

Electrical and thermal properties

The HOMO level of the three materials was measured using ultraviolet photoelectron spectroscopy (UPS), and the LUMO levels were determined from the HOMO level and the optical band gap. The optical band gaps were derived by determining the absorption

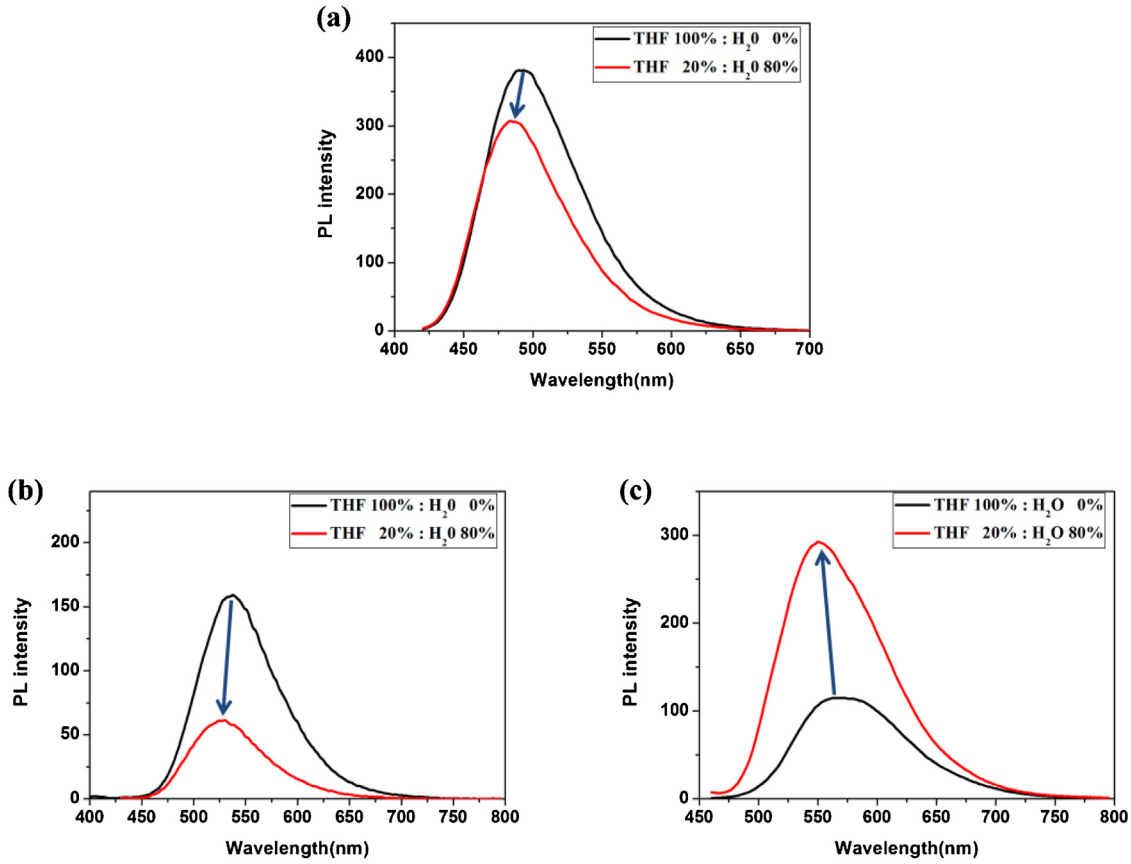

Fig. 5. Simple aggregation-induced emission test of synthesized compounds. (a) DPAT-Ph. (b) DPAT-Na. (c) DPAT-An.

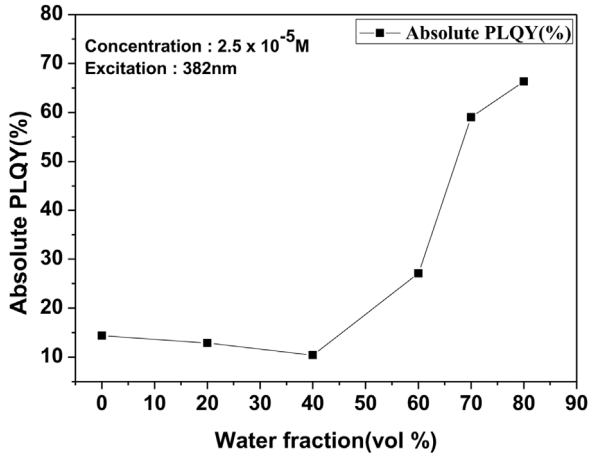

Fig. 6. The dependence of the absolute PLQY of DPAT-An in a THF:H_2O mixture on the amount of water in the mixture.

edges from plots of $(h\nu)$ versus $(\alpha h\nu)^2$, where α, h, and ν are the absorbance, Planck's constant, and the frequency of light, respectively. The HOMO levels, LUMO levels, and band gaps are summarized in Table 2. The HOMO level of DPAT-Ph, DPAT-Na, and DPAT-An is −5.66, −5.67, and −5.65 eV, respectively, and the LUMO level is −2.83, −3.05, and −3.19 eV. The corresponding band gaps were 2.83, 2.62, and 2.46 eV, respectively. The decreased band gap of the compounds matched the decrease of band gap of the core groups and the band gap of benzene, naphthalene, and anthracene is 6.72, 4.75, and 3.58 eV, respectively [26,27].

To evaluate the thermal properties of the synthesized compounds, thermogravimetric analysis (TGA) and differential scanning calorimetry (DSC) were performed. In the TGA analysis, the decomposition temperature (T_d) was defined as the temperature at 5% weight loss temperature. The T_d value of DPAT-Ph, DPAT-Na, and DPAT-An was 342, 365, and 370 °C, respectively (Fig. S4(a)). The T_d value increased as the core group changed from phenyl to anthracene because the molecular weight increased. When the materials were analyzed with DSC, a second heating was performed to determine clearly the glass transition temperature (T_g). DPAT-Ph, DPAT-Na, and DPAT-An exhibited T_g values of 68, 89, and 242 °C, respectively Fig. S4(b). Generally, the thermal properties of materials used in OLED devices are related to device lifetime because Joule heating occurs during operation of OLED devices, and that can change the morphology of the materials and even degrade the materials [28]. Thus, DPAT-An with a relatively higher thermal stability could be expected to possess a superior device lifetime in an optimized OLED device.

Electroluminescent properties

To investigate the EL properties of the synthesized materials, OLED devices were fabricated. The synthesized materials were used as the emitting layer (EML) in the OLED devices. The device structure consisted of a stack of the following layers: indium tin oxide (ITO)/tris(N-(naphthalen-2-yl)-N-phenyl-amino)triphenyl-amine (2-TNATA, 60 nm)/N,N′-bis(naphthalen-1-yl)-N,N′-bis(phenyl)benzidine (NPB, 15 nm)/the synthesized compounds (30 nm)/1,3,5-tris(phenyl-2-benzimidazolyl)benzene (TPBi, 30 nm)/LiF (1 nm)/Al (200 nm). 2-TNATA was used as a hole injection layer (HIL), NPB was used as a hole transporting layer (HTL), and TPBi was used as an electron transporting layer (ETL) and a hole blocking layer. The properties of the fabricated OLED devices are summarized in Table 3 and Fig. 7. shows their *I–V–L* curves and

Table 3
OLED device performance of synthesized compounds.

Device 10 mA/cm^2	Operating voltage (V)	Luminance efficiency (cd/A)	Power efficiency (lm/W)	E.Q.E. (%)	CIE(x, y)	EL_{max} (nm)
DPAT-Ph	6.29	3.71	2.07	3.61	(0.14, 0.19)	469
DPAT-Na	7.15	8.09	3.74	3.10	(0.22, 0.54)	502
DPAT-An	7.62	17.97	8.20	5.20	(0.40, 0.57)	547
Alq_3	6.32	4.73	2.7	1.77	(0.33, 0.54)	510

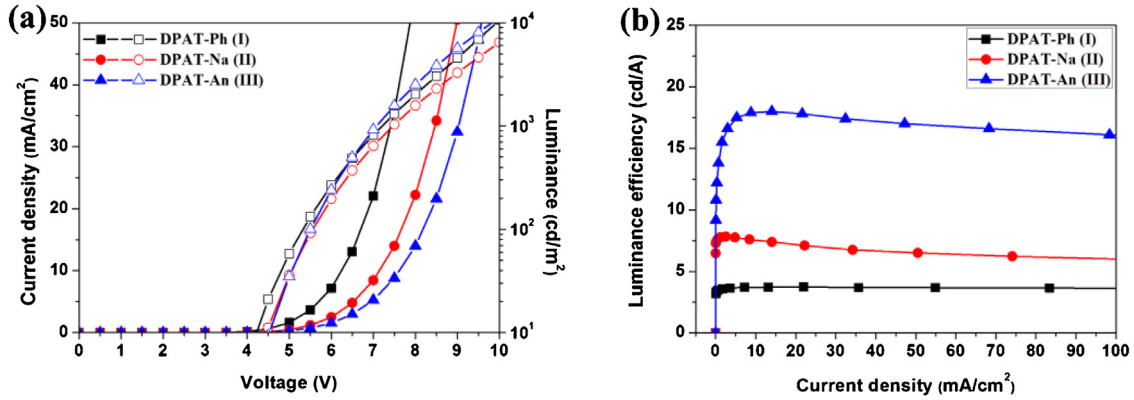

Fig. 7. OLED device performance of synthesized compounds. (a) *I–V–L* curves versus voltage. (b) Luminance efficiency versus current density.

luminance efficiency (LE) values. As shown in Table 3, the EL maximum wavelengths (EL_{max}) were 469, 502, and 547 nm, respectively, and these wavelengths were similar to the PL_{max} values in the film state. The similarity means that the charge recombination zone was positioned in the EML. In Table 3 and Fig. 7(b), remarkable points are LE values of three materials at 10 mA/cm^{-2}. DPAT-Ph, DPAT-Na, and DPAP-An had LE values of 3.71, 8.09, and 17.97 cd/A, respectively. Except the DPAT-Ph exhibiting sky-blue emission, DPAT-Na and DAPT-An exhibiting green emission shows LE value 1.7 times higher or 3.8 times higher than Alq_3, which is standard green fluorescence material, respectively. These high LE values resulted from efficient charge recombination due to the bipolar structure of the synthesized compounds. As seen in Fig. S5, depending on the lowered LUMO levels of the three materials, the barrier was increased between the LUMO level of the EML and the LUMO level of the HTL, and electrons from the ETL could be efficiently blocked in the EML. Thus, among the three materials, DPAT-An, which had the lowest LUMO level, could efficiently block electrons between the HTL and EML, an advantage in that the recombination zone was confined to the EML. Also, the differences of LE values could be understood by comparing the core groups. The OLED devices had a higher LE value when the anthracene, which had a relatively higher PLQY value than the other core groups, was used as the core group than when the phenyl or naphthyl groups were used.

It is possible that another reason why DPAT-An had a high LE value was the AIE phenomenon. Because DPAT-Ph and DPAT-Na do not exhibit the AIE phenomenon, their absolute PLQY values in the film state were relatively lower than in the solution state. However, because DPAT-An exhibited the AIE phenomenon, its absolute PLQY value in the film state was higher than that in solution state, and DPAT-An showed the highest absolute PLQY value in the film state. Thus, the AIE phenomenon helped increase EL efficiency of the OLED device, and DPAT-An exhibited the highest LE value of 17.97 cd/A among the three materials.

Looking at the external quantum efficiency (EQE) values, DPAT-Ph, DPAT-Na, and DPAT-An shows the EQE value of 3.61%, 3.10%, and 5.20%, respectively. Only DPAT-An exhibits the EQE value of over 5%, which is a value exceeding the theoretical limitation of fluorescence OLED. This phenomenon might be thought that it is originated from delayed fluorescence by triplet-triplet annihilation (TTA) because anthracene derivatives are well-known to show TTA phenomenon [10,29–31].

Comparing with the previous studies, 10-(3,5-diphenylphenyl)-N,N-diphenylanthracen-9-amine (MADa) and 3-(10-(4,6-diphenyl-1,3,5-triazin-2-yl)anthracen-9-yl)-9-phenyl-9H-carbazole (3CzAnTrz) showed the EL_{max} of 497, 488 nm and the LE value of 10.3, 13.34 cd/A, respectively [32,33]. The EL_{max} of DPAT-An was 50–60 nm red-shifted, the LE value of DPAT-An was 17.97 cd/A, which is 1.3 times or 1.7 times higher value compared to the previous studies. This is due to an efficient charge recombination based on the bipolar characteristics by DPA moiety and DPT-moiety.

To evaluate the stability of the fabricated OLED devices, device lifetime was measured at 1000 cd/m^2. As seen in Fig. 8, among the three synthesized compounds, DPAT-An exhibited the longest device lifetime of 1310 h. Significantly, the OLED device based on DPAT-An exhibited a longer device lifetime than the same OLED device based on Alq_3. It can be thought that increased device

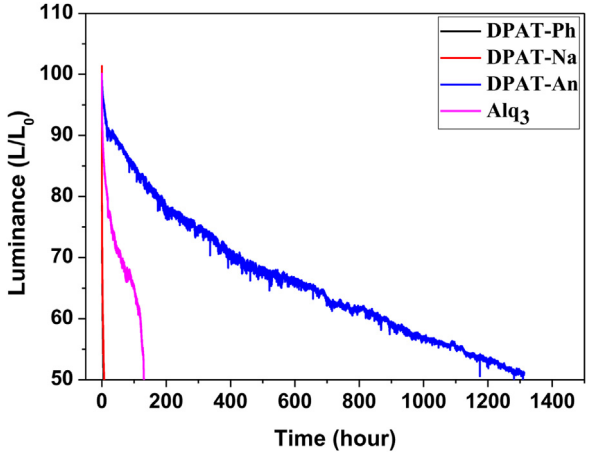

Fig. 8. Lifetime data of fabricated OLED devices.

lifetime was resulted from relatively reduced Joule heating, which is resulted from the decreased amount of injected current at same brightness by high LE value. The synthesized materials did not undergo a sublimation process, and green OLED devices with long device lifetime can be fabricated by using standard equipment. This is due to the use of robust organic green emitters under electric fields.

Conclusions

Three bipolar materials were successfully synthesized and characterized. Of the three materials, DPAT-An had a highly twisted structure. Due to the bipolar nature of the synthesized compounds, their PL_{max} values were red-shifted according to increased solvent polarity. Significantly, DPAT-An exhibited the AIE phenomenon. DPAT-An had a very weak PL emission in the solution state but a very strong PL emission of 64% PLQY in the film state. In an OLED device, DPAT-Ph, DPAT-Na, and DPAT-An had EL maximum wavelengths of 469, 502, and 547 nm, respectively. DPAT-An, exhibiting the AIE phenomenon, had a very high LE of 17.97 cd/A and a long OLED device lifetime of 1310 h. Thus, an OLED device with high efficiency and long lifetime can be realized through bipolar molecular design, which can result in efficient charge recombination and the AIE phenomenon.

Conflict of interest

None declared.

Acknowledgements

This research was supported by National R&D Program through the National Research Foundation of Korea (NRF) funded by the Ministry of Science & ICT (No. 2017M3A7B4041699). This research was supported by the Basic Science Research Program through the National Research Foundation of Korea (NRF) funded by the Ministry of Education (Nos. 2017R1D1A1A09082138 and 2018R1A6A1A03023788). This work was supported by Institute for Basic Science (IBS-R004).

Appendix A. Supplementary data

Supplementary data associated with this article can be found, in the online version, at https://doi.org/10.1016/j.jiec.2020.04.003.

References

[1] C.W. Tang, S.A. Van Slyke, Appl. Phys. Lett. 51 (1987) 913, doi:http://dx.doi.org/10.1063/1.98799.
[2] N.S. Baek, S.K. Hau, H.L. Yip, O. Acton, K.S. Chen, A.K.Y. Jen, Chem. Mater. 20 (2008) 5734, doi:http://dx.doi.org/10.1021/cm8016424.
[3] I. Kang, J.-A. Hong, R. Kim, J.-W. Jang, J. Hwang, J.H. Kim, S.-K. Kwon, Y.-H. Kim, Macromol. Res. 21 (2013) 450, doi:http://dx.doi.org/10.1007/s13233-013-1044-3.
[4] C.W. Tang, S.A. Van Slyke, C.H. Chen, J. Appl. Phys. 65 (1989) 3610, doi:http://dx.doi.org/10.1063/1.343409.
[5] M.A. Baldo, M.E. Thompson, S.R. Forrest, Nature 403 (2000) 750, doi:http://dx.doi.org/10.1038/35001541.
[6] C.-C. Wu, Y.-T. Lin, K.-T. Wong, R.-T. Chen, Y.-Y. Chien, Adv. Mater. 16 (2004) 61, doi:http://dx.doi.org/10.1002/adma.200305619.
[7] C. Adachi, T. Tsutsui, S. Saito, Appl. Phys. Lett. 55 (1989) 1489, doi:http://dx.doi.org/10.1063/1.101586.
[8] S.-K. Kim, Y.-I. Park, I.-N. Kang, J.-W. Park, J. Mater. Chem. 17 (2007) 4670, doi:http://dx.doi.org/10.1039/B706606F.
[9] S.-K. Kim, B. Yang, Y. Ma, J.-H. Lee, J.-W. Park, J. Mater. Chem. 18 (2008) 3376, doi:http://dx.doi.org/10.1039/B805062G.
[10] B. Kim, Y. Park, J. Lee, D. Yokoyama, J.H. Lee, J. Kido, J. Park, J. Mater. Chem. C 1 (2013) 432, doi:http://dx.doi.org/10.1039/C2TC00185C.
[11] J. Luo, Z. Xie, J.W.Y. Lam, L. Cheng, H. Chen, C. Qiu, H.S. Kwok, X. Zhan, Y. Liu, D. Zhu, B.Z. Tang, Chem. Commun. (2001) 1740, doi:http://dx.doi.org/10.1039/B105159H.
[12] J. Mei, N.L.C. Leung, R.T.K. Kwok, J.W.Y. Lam, B.Z. Tang, Chem. Rev. 115 (2015) 11718, doi:http://dx.doi.org/10.1021/acs.chemrev.5b00263.
[13] Y. Dong, J.W.Y. Lam, A. Qiu, J. Sun, J. Liu, Z. Li, S. Zhang, J. Sun, H.S. Kwok, B.Z. Tang, Appl. Phys. Lett. 91 (2007) 011111, doi:http://dx.doi.org/10.1063/1.2753723.
[14] Z. Zhao, S. Chen, J.W.Y. Lam, P. Lu, Y. Zhong, K.S. Wong, H.S. Kwok, B.Z. Tang, Chem. Commun. 46 (2010) 2221, doi:http://dx.doi.org/10.1039/B921451H.
[15] Z. Zhao, P. Lu, J.W.Y. Lam, Z. Wang, C.Y.K. Chan, H.H.Y. Sung, I.D. Williams, Y. Ma, B.Z. Tang, Chem. Sci. 2 (2011) 672, doi:http://dx.doi.org/10.1039/C0SC00521E.
[16] Z. Zhao, S. Chen, J.W.Y. Lam, Z. Wang, P. Lu, M. Faisal, H.H.Y. Sung, I.D. Williams, Y. Ma, H.S. Kwok, B.Z. Tang, J. Mater. Chem. 21 (2011) 7210, doi:http://dx.doi.org/10.1039/C0JM04449K.
[17] Z. Zhao, S. Chen, C.Y.K. Chan, J.W.Y. Lam, C.K.W. Jim, P. Lu, Z. Chang, H.S. Kwok, H. Qiu, B.Z. Tang, Chem. Asian J. 7 (2012) 484, doi:http://dx.doi.org/10.1002/asia.201100753.
[18] Z. Chang, Y. Jiang, B. He, J. Chen, Z. Yang, P. Lu, H.S. Kwok, Z. Zhao, H. Qiu, B.Z. Tang, Chem. Commun. 49 (2013) 594, doi:http://dx.doi.org/10.1039/C2CC37928G.
[19] C.H. Chang, M.C. Kuo, W.C. Lin, Y.T. Chen, K.T. Wong, S.H. Chou, E. Mondal, R.C. Kwong, S. Xia, T. Nakagawa, C. Adachi, J. Mater. Chem. 22 (2012) 3832, doi:http://dx.doi.org/10.1039/C2JM14686J.
[20] A. Benor, S.Y. Takizawa, C. Perez Bolivar, P. Anzenbacher, Appl. Phys. Lett. 96 (2010) 243310, doi:http://dx.doi.org/10.1063/1.3452344.
[21] S. Lee, K.-H. Kim, D. Limbach, Y.-S. Park, J.-J. Kim, Adv. Funct. Mater. 23 (2013) 4105, doi:http://dx.doi.org/10.1002/adfm.201300187.
[22] S. Gong, Y. Chen, J. Luo, C. Yang, C. Zhong, J. Qin, D. Ma, Adv. Funct. Mater. 21 (2011) 1168, doi:http://dx.doi.org/10.1002/adfm.201002066.
[23] J.H. Huang, J.H. Su, X. Li, M.K. Lam, K.M. Fung, H.H. Fan, K.W. Cheah, C.H. Chen, H.J. Tian, J. Mater. Chem. 21 (2011) 2957, doi:http://dx.doi.org/10.1039/C0JM03300F.
[24] M.J. Frisch, G.W. Trucks, H.B. Schlegel, G.E. Scuseria, M.A. Robb, J.R. Cheeseman, G. Scalmani, V. Barone, B. Mennucci, G.A. Petersson, H. Nakatsuji, M. Caricato, X. Li, H.P. Hratchian, A.F. Izmaylov, J. Bloino, G. Zheng, J.L. Sonnenberg, M. Hada, M. Ehara, K. Toyota, R. Fukuda, J. Hasegawa, M. Ishida, T. Nakajima, Y. Honda, O. Kitao, H. Nakai, T. Vreven, J.A. Montgomery, J.E. Peralta Jr., F. Ogliaro, M. Bearpark, J.J. Heyd, E. Brothers, K.N. Kudin, V.N. Staroverov, R. Kobayashi, J. Normand, K. Raghavachari, A. Rendell, J.C. Burant, S.S. Iyengar, J. Tomasi, M. Cossi, N. Rega, J.M. Millam, M. Klene, J.E. Knox, J.B. Cross, V. Bakken, C. Adamo, J. Jaramillo, R. Gomperts, R.E. Stratmann, O. Yazyev, A.J. Austin, R. Cammi, C. Pomelli, J.W. Ochterski, R.L. Martin, K. Morokuma, V.G. Zakrzewski, G.A. Voth, P. Salvador, J.J. Dannenberg, S. Dapprich, A.D. Daniels, Ö. Farkas, J.B. Foresman, J.V. Ortiz, J. Cioslowski, D.J. Fox, Gaussian 09 Revision D.1, Gaussian, Inc., Wallingford, CT, 2009.
[25] M. Chen, H. Nie, B. Song, L. Li, J.Z. Sun, A. Qin, B.Z. Tang, J. Mater. Chem. C 4 (2016) 2901, doi:http://dx.doi.org/10.1039/C5TC03299G.
[26] P. Masiak1, M. Wierzbowska, J. Mater. Sci. 52 (2017) 4378, doi:http://dx.doi.org/10.1007/s10853-016-0685-y.
[27] J.C.S. Costa, R.J.S. Taveira, C.F.R.A.C. Lima, A. Mendes, L.M.N.B.F. Santos, Opt. Mater. 58 (2016) 51, doi:http://dx.doi.org/10.1016/j.optmat.2016.03.041.
[28] Y. Park, B. Kim, C. Lee, A. Hyun, S. Jang, J.-H. Lee, Y.-S. Gal, T.H. Kim, K.-S. Kim, J. Park, J. Phys. Chem. C 115 (2011) 4843, doi:http://dx.doi.org/10.1021/jp108719w.
[29] C.A. Parker, T.A. Joyce, Chem. Commun. 6 (1967) 744, doi:http://dx.doi.org/10.1039/C19670000744.
[30] D. Yokoyama, Y. Park, B. Kim, S. Kim, Y.-J. Pu, J. Kido, J. Park, Appl. Phys. Lett. 99 (2011) 123303, doi:http://dx.doi.org/10.1063/1.3637608.
[31] S. Kang, H. Jung, H. Lee, S. Park, J. Kim, J. Park, J. Mater. Chem. C 7 (2019) 14709, doi:http://dx.doi.org/10.1039/C9TC04603H.
[32] S.-K. Kim, B. Yang, Y.-I. Park, Y. Ma, J.-Y. Lee, H.-J. Kim, J. Park, Org. Electron. 10 (2009) 822, doi:http://dx.doi.org/10.1016/j.orgel.2009.04.003.
[33] W. Liu, S. Ying, Q. Zhang, S. Ye, R. Guo, D. Ma, L. Wang, Dyes Pigm. 158 (2018) 204, doi:http://dx.doi.org/10.1016/j.dyepig.2018.05.030.